Supporting Information for:

Delocalization Tunable by Ligand Substitution in [L$_2$Al]$^{n-}$ Complexes Highlights a Mechanism for Strong Electronic Coupling

Amela Arnold, Tobias J. Sherbow, Amanda M. Bohanon, Richard I. Sayler, R. David Britt, Allison M. Smith, James C. Fettinger, and Louise A. Berben*

Department of Chemistry, University of California, Davis CA 95616

Table of Contents

1. Experimental Methods

Physical Measurements. ^{1}H, ^{19}F and ^{13}C NMR spectra were recorded at ambient temperature using a Varian 600 MHz or a Bruker 400 MHz spectrometer. Chemical shifts were referenced to residual solvent. GC-MS measurements were conducted on Agilent 6890N GC with a 5973N MSD and a Varian FactorFour Capillary Column (VF-5ms, 30 m × 0.25 mM ID DF = 0.25). Elemental analyses were performed by the Microanalytical Laboratory at The University of California, Berkeley. For HRMS analysis, samples were analyzed by flow-injection analysis into a Thermo Fisher Scientific LTQ Orbitrap XL (San Jose, CA) operated in the centroided mode. Samples were injected into a mixture of 50% MeOH and 0.1% Formic Acid/H20 at a flow of 200 ul/min. Source parameters were 5kV spray voltage, capillary temperature of 275°C and sheath gas setting of 20. Spectral data were acquired at a resolution setting of 100,000 FWHM with the lockmass feature which typically results in a mass accuracy < 2 ppm.

Cyclic voltammograms (CVs) were recorded in a nitrogen atmosphere using Schlenk air-free techniques. A CH Instruments Electrochemical Analyzer Model 620D with a glassy carbon working electrode (CH Instruments, nominal surface area of 0.071 cm^2), a platinum wire auxiliary electrode, and an Ag/AgNO$_3$ (0.001M) non-aqueous reference electrode with a Vycor tip. All potentials are referenced to the SCE couple, and ferrocene was used as an external standard where the E$_{\frac{1}{2}}$ of ferrocene/ferrocenium is +0.56 V vs. SCE in 0.3 M Bu$_4$NPF$_6$ THF or +0.40 V vs. SCE in 0.1 M Bu$_4$NPF$_6$ MeCN.[1] Bu$_4$NPF$_6$ was recrystallized from ethanol and placed under vacuum for 72 hours before electrolyte solutions were made. Electrolyte solutions were stored over 3 Å molecular sieves for at least 48 hours before use. Sieves were activated by heating under vacuum at 270°C for at least 72 hours.

UV-Vis-NIR spectra were obtained using a 1 cm cuvette using a Lambda 750 UV-Vis-NIR spectrophotometer and Shimadzu UV-Vis-NIR spectrophotometer. NIR spectroscopic samples were prepared in a nitrogen filled glovebox in 1 mm quartz cuvettes. Estimation of the full bandwidth at half maximum for the NIR IVCT bands was performed using data that was plotted as extinction coefficient vs absorption wavenumber (ε versus ν). Gaussian fits were obtained with non-linear iterative curve fitting using the nonlinear least square (NLS) function in R.[2,3] For highly reduced **A**$^{2-}$, the Gaussian fit was performed on the higher-energy portion of the distribution. When Gaussian distributions are truncated on the lower-energy side, primarily for Class II/III borderline systems, metrics necessary for IV-CT Hush analysis are extracted from the high-energy fit.[4]

Electron paramagnetic resonance (EPR) spectroscopy. Electron paramagnetic resonance (EPR) spectroscopy was performed in the CalEPR center in the Department of Chemistry, University of California at Davis. All EPR samples were prepared in toluene or THF with a concentration of 1 mM the respective complex. X-band (9.4 GHz) continuous-wave (CW) EPR spectra were recorded on a Bruker ELEXSYS E500 spectrometer equipped with a cylindrical TE011-mode resonator (SHQE-W), an ESR 900-liquid helium cryostat, and an ITC-5 temperature controller (Oxford Instruments). All CW EPR spectra were recorded at slow-passage, non-saturating conditions. Experimental parameters including temperature and solvent were varied in an attempt to resolve hyperfine coupling and to obtain more details from the EPR spectra, but we have so far been unsuccessful in obtaining better spectra.

On the EPR time scale of 10^{-7}-10^{-10}, the X-band cwEPR spectrum of **2** is inconclusive with respect to delocalization (Figure S17 right). The linewidth is narrow (4.1 mT) relative to **1** (7.2 mT). The lack of resolved hyperfine coupling for **2** precludes the assignment of electron localization based on the EPR, but loss of resolved hyperfine coupling and line narrowing could be consistent with increased delocalization.[5] However, the timescale and standard functionals of the EPR experiment tend to overestimate delocalization due to the self-interaction error: Class II MV compounds often appear delocalized when probed using EPR. Therefore, the EPR results obtained here are consistent with the NIR data collected for **2**, which suggests a Class II/III system, although they do not add any further insights. Instability of solutions of (K:18-C-6)$_2$-**2**, **3** and (K:18-C-6)$_2$-**3** prevented acquisition of EPR data for those compounds.

X-ray Structure determinations. X-ray diffraction studies were carried out on a Bruker SMART APEXII, and a Bruker Photon100 CMOS diffractometer equipped with a CCD detector.[6a] Measurements were carried out at 90 K using Mo Kα ($\lambda = 0.71073$ Å) and Cu Kα (1.5418 Å) radiation. Crystals were mounted on a Kaptan Loop with Paratone-*N* oil. Initial lattice parameters were obtained from a least-squares analysis of more than 100 centered reflections; these parameters were later refined against all data. Data were integrated and corrected for Lorentz polarization effects using SAINT,[3b] and were corrected for absorption effects using SADABS2.3.[3c]

Space group assignments were based upon systematic absences, *E* statistics, and successful refinement of the structures. Structures were solved by direct methods with the aid of successive difference Fourier maps and were refined against all data using the SHELXTL 5.0 software package.[1d] Thermal parameters for all non-hydrogen atoms were refined anisotropically. Hydrogen atoms, where

added, were assigned to ideal positions and refined using a riding model with an isotropic thermal parameter 1.2 times that of the attached carbon atom (1.5 times for methyl hydrogens).

Preparation of Compounds. All manipulations were carried out using standard Schlenk or glove-box techniques under a dinitrogen atmosphere. Unless otherwise noted, solvents were deoxygenated and dried by thorough sparging with Ar gas followed by passage through an activated alumina column. Deuterated solvents were purchased from Cambridge Isotopes Laboratories, Inc. and were degassed and stored over activated 3 Å molecular sieves prior to use. 2,6-dibenzoylpyridine,[7] and **1**,[8] were synthesized according to a modified version of the literature. All other reagents were purchased from commercial vendors and used without further purification.

2,6-Bis{1-[(perfluorophenyl)imino]-benzyl}pyridine ligand ($_{F5}$I$_2$P). A modified Schiff base condensation reaction to form $_{F5}$I$_2$P was performed as follows: 2,6-dibenzoylpyridine (2.00 g, 6.96 mmol), 2.5 equivalents of pentafluoroaniline (3.19 g, 17.4 mmol), and a catalytic quantity of tosic acid (0.012 g) was dissolved in 70 mL of dry toluene. The mixture was refluxed with a Dean-Stark trap for 25 h. The brown-red solution was cooled and concentrated to a brown oil. The oil was triturated with 50 mL of hexanes, resulting in a fine yellow powder, which was filtered. The powder was washed with fresh hexanes and dried on a high vacuum line overnight: 3.54 g, 82%; ^{1}H NMR (C$_6$D$_6$, 298K, 400 MHz): δ 8.36 (d, $J = 8$ Hz, 1H, py), 8.14 (d, $J = 8$ Hz, 1H, py), 7.62-7.57 (m, 4H, py), 7.21 (t, $J = 8$ Hz, 1H, py), 7.13-6.69 (m, 20H, aryl), 6.61-6.55 (m, 1H, aryl) (The system has a series of different isomers). HRMS (ESI/ion trap) m/z: [M + H]$^+$ Calcd: 618.0983; Found: 618.1001. ^{13}C NMR (C$_6$D$_6$, 298K, 150 MHz): δ 176.22, 176.11, 173.11, 172.23, 155.47, 154.77, 154.53, 153.22, 139.02, 137.90, 137.60, 137.15, 136.93, 135.41, 135.05, 132.99, 132.51, 130.55, 130.49, 130.10, 129.64, 129.03, 128.94, 128.69, 128.47, 128.12, 127.65, 126.69, 125.57, 124.81, 123.93. ^{19}F NMR (376.5 MHz, C$_6$D6): δ -151.46, -151.48, -151.52, -151.54, -151.59, -151.60, -151.64, -151.65, -151.70, -151.71, -152.03, -152.05, -152.06, -152.09, -152.10, -152.11, -152.12, -162.14, -162.20, -162.26, -162.26, -162.40, -162.46, -162.46, -162.51, -162.51, -162.52, -163.25, -163.31, -163.32, -163.37, -163.38, -163.46, -163.48, -163.52, -163.54, -163.58, -163.59, -163.63, -163.65, -163.67, -163.68, -163.69, -163.71, -163.73, -163.74, -163.75, -163.79, -163.80, -163.81, -163.94, -163.95, -163.96, -164.00, -164.01, -164.03, -164.06, -164.07, -164.08, -164.25, -164.26, -164.31, -164.32, -164.37, -164.38. UV-vis-NIR spectrum (THF) λ_{max} (ε_M): 351 (2840) nm (L mol^{-1} cm^{-1}).

2,6-Bis{3-[(N,N-dimethylaniline)imino]-benzyl}pyridine ligand ($_{NMe2}$I$_2$P). Condensation of 2,6-dibenzoylpyridine with excess *N,N*-dimethyl-*p*-phenylenediamine was performed by first dissolving 2,6-dibenzoylpyridine (1.00 g, 3.48 mmol), three equivalents of *N,N*-dimethyl-*p*-phenylenediamine (1.50 g, 11.01 mmol), and a catalytic quantity of tosic acid (0.0070 g, 0.0368 mmol) in 70 mL of dry toluene. The mixture was refluxed with a Dean-Stark trap for 6 days. Reaction progress was monitored through GC-MS. The brown-red solution was cooled and concentrated *in vacuo*. Solids were stirred in a toluene (5 mL): hexanes (50 mL) mixture and filtered to remove unreacted aniline. The orange solids were precipitated out of solution by adding methanol (10 mL). Recrystallization from dry ether resulted in orange crystalline needles: 1.00 g, 55% yield. HRMS (ESI/ion trap) m/z: [M + H]$^+$

Calcd: 524.2809; Found: 524.2807. ^{1}H and ^{13}C NMR displays three constitutional isomers in 45%, 35% and 20% abundance for the (*Z,Z*), (*E,Z*) and (*E,E*) isomers, respectively. The following NMR data provided are for the (*Z,Z*) isomer. ^{1}H NMR (600 MHz, C_6D_6): δ 8.00 (d, J = 7.8, 4H, Ar), 7.18 – 6.85 (m, 7H, py and Ar), 6.55 (m, 2H, Ar), 6.45 (d, J = 8.6, 4H, Ar), 6.34 (t, J = 8.6, 4H, Ar), 2.42 (s, 12H, N*Me$_2$*). ^{13}C NMR (C_6D_6, 298K, 151 MHz): δ 164.29, 156.69, 147.41, 141.11, 139.17, 135.75, 130.15, 130.04, 129.97, 129.02, 127.92, 127.90, 127.27, 124.01, 123.84, 123.43, 123.25, 123.05, 112.62, 112.54, 112.40, 112.38, 40.04, 40.02, 39.81, 39.79. UV-vis-NIR spectrum (THF) λ_{max} (ε_M): 409 (7300), nm (L mol^{-1} cm^{-1}).

($_{F5}I_2P^-$) ($_{F5}I_2P^{2-}$)Al (**2**). The $_{F5}I_2P$ ligand (2 equiv, 0.162 mmol, 100 mg) was dissolved in 5 mL THF. In a separate vial, AlCl$_3$ (1 equiv, 0.081 mmol, 10.8 mg) was dissolved in 2 mL THF. The AlCl$_3$ in THF was added to the $_{F5}I_2P$ ligand dropwise. A slight color change from yellow-orange to bright yellow was observed. This was allowed to stir for ten minutes, after which solid sodium (3.2 equiv, 0.260 mmol, 6 mg) was added to the slurry. This was stirred for three days at room temperature, at which point a red-brown slurry formed. This was filtered through a celite pad and the brown solution was concentrated to dryness. Crystals suitable for X-ray diffraction were grown by layering hexane into a concentrated ether solution and storing at -20°C over three days (52% yield). HRMS (ESI/ion trap) m/z: [M]$^+$ Calcd for $C_{62}H_{26}AlF_{20}N_6$ 1261.1715; Found 1261.1694. UV-vis-NIR spectrum (benzene) λ_{max} (ε_M): 345 (sh, 22 400), 435 (sh, 12 400), 505 (sh, 8620), 1315 (3410), 1655 (2640) nm (L mol^{-1} cm^{-1}). Magnetic Moment (Evan's Method): μ_{eff} = 2.06 B.M. Anal. Calcd. for $C_{62}H_{26}AlF_{20}N_6 \cdot C_6H_6 \cdot C_6H_{14}$: C, 62.30; H, 3.25; N, 5.89. Found: C, 62.60; H, 3.53; N, 5.92.

($_{NMe2}I_2P^-$) ($_{NMe2}I_2P^{2-}$)Al (**3**). The $_{NMe2}I_2P$ ligand (0.1 g, 0.1910 mmol) was dissolved in 5 mL THF. Solid sodium (0.0068 g, 0.2960 mmol) was added and the solution was stirred at room temperature for 3 days, during which the solution color changed from yellow-orange to dark red-purple. A solution of AlCl$_3$ (0.0127 g, 0.0955 mmol) in THF (2 mL) was added. This dark reddish solution was stirred for 15 minutes, then concentrated down *in vacuo*, yielding a brown-red solid. The solids were dissolved in benzene and filtered through celite to remove salts. The complex was recrystallized at room temperature overnight from a slow diffusion of pentane into a concentrated solution of the complex in benzene, yielding red rod crystals suitable for X-ray diffraction, 15.4 mg, 15%. HRMS (ESI/ion trap) m/z: [M/3]$^+$ Calcd. for $C_{70}H_{66}AlN_{10}$ 357.8429; Found 357.8416. UV-vis-NIR spectrum (benzene) λ_{max} (ε_M): 410 (29

600), 550 (sh, 14 500), 1466 (4390), 1936 (3880) nm (L mol^{-1} cm^{-1}). μ_{eff} = 1.60 μ_B. This compound decomposed during the multiple recrystallizations required to make it pure enough for combustion analysis and so no analysis is available. It is for this reason that we synthesized $\mathbf{3}^{2+}$ to use as a precursor from which to generate **3** and $\mathbf{3}^{2-}$ for the UV-Vis-NIR studies.

[($_{NMe2}$I$_2$P$^-$)$_2$Al][OTf]$_2$ ($\mathbf{3}^{2+}$). Two equivalents of the $_{NMe2}$I$_2$P ligand (96.2 mg, 0.184 mmol) was dissolved in 5 mL THF. Solid sodium (4.4 mg, 0.193 mmol) was added and the solution was stirred at room temperature overnight, during which the solution color changed from yellow-orange to dark green. A solution of AlCl$_3$ (12.2 mg, 0.092 mmol) in THF (2 mL) was added. This dark reddish solution was stirred for 15 minutes, then potassium trifluoromethanesulfonate (19.0 mg, 0.101 mmol) was added as a solid. This solution was stirred overnight and then concentrated *in vacuo*, yielding a red solid. The solids were triturated with benzene (3 x 5 mL) and filtered through celite. The filtrate was discarded and the oily red solids were dissolved in acetonitrile and filtered through the same celite pad. This solution was concentrated, yielding dark red solids (36.7 mg, 33% yield). The complex was purified from a slow diffusion of pentane into a concentrated solution of the complex in THF at -20°C, yielding red solids. HRMS (ESI/ion trap) m/z: [M/3]$^{3+}$ Calcd. for C$_{70}$H$_{66}$AlN$_{10}$ 357.8433; Found 357.8424. [M/2 + H]$^{2+}$ Calcd. for C$_{70}$H$_{66}$AlN$_{10}$ 537.7716; Found 537.7703. UV-vis-NIR spectrum (THF) λ_{max} (ε_M): 407 (12 500), 481 (16 800), 1969 (3560) nm (L mol^{-1} cm^{-1}). μ_{eff} = 1.73 μ_B. Anal. Calcd. for C$_{72}$H$_{66}$AlF$_6$N$_{10}$O$_6$S$_2$·2H$_2$O: C, 61.40; H, 5.01; N, 9.94. Found: C, 61.45; H, 4.97; N, 9.85.

($_{F5}$I$_2$P$^-$)AlCl$_2$ (4). One equivalent of the $_{F5}$I$_2$P ligand (200 mg, 0.324 mmol) in THF (4 mL) was added dropwise to one equivalent of AlCl$_3$ (43.2 mg, 0.324 mmol) in THF (2 mL). Solid sodium (7.8 mg, 0.34 mmol) was added to this yellow solution. The reaction was stirred for 24 h until the solution was a uniform green-red color. The THF solvent was removed *in vacuo.* The brown solid was triturated with benzene (5 mL), and the solution was discarded. The remaining solids were dissolved in THF (2 mL) and recrystallized by slow diffusion of pentane into the concentrated THF solution at room temperature (162 mg, 70%). UV-vis-NIR spectrum (benzene) λ_{max} (ε_M): 348 (3090), 463 (sh, 1120), 1006 (147), 1310 (486), 1656 (780) nm (L mol^{-1} cm^{-1}). μ_{eff} = 1.40 μ_B. Anal. Calcd. for C$_{31}$H$_{13}$AlCl$_2$F$_{10}$N$_3$·C$_4$H$_8$O: C, 53.36; H, 2.69; N, 5.34. Found: C, 53.31; H, 2.52; N, 5.24.

($_{F5}$I$_2$P^{2-})AlCl(THF)$_2$ (5). Solid sodium (32 mg, 1.39 mmol) was stirred with $_{F5}$I$_2$P (414 mg, 0.67 mmol) and AlCl$_3$ (94 mg, 0.69 mmol) in THF (5 mL) until the sodium was consumed (up to one week).

Volatiles were removed under vacuum and the product was extracted into benzene, filtered over Celite to remove salts, and the solvent was removed *in vacuo*, to give **5** (480 mg, 87%). Crystals suitable for X-ray diffraction were grown by slow diffusion of hexanes into a THF solution of **5** at -25 ℃ overnight. ^{1}H-NMR (600 MHz, C_6D_6): δ 7.30-6.80 (m, 10H, Ar), 6.30 (br, 2H, py), 5.30 (t, J = 7.4 Hz, 1H, py), 3.61 (br, 4H, THF) ppm. ^{13}C NMR (151 MHz, C_6D6) δ 147.41, 144.42, 142.81, 139.39, 139.30 (t, J = 10.8 Hz), 138.86 (t, J = 14.5 Hz), 137.65 (t, J = 13.2 Hz), 137.21 (t, J = 14.7 Hz), 134.65, 133.59, 128.48, 125.83, 120.17, 72.24, 25.27. ^{19}F-NMR (376 MHz): δ -148.87 (m, 2F), -161.05 (t, J = 22 Hz, 1F), -165.57 (m, 2F). UV-vis-NIR spectrum (benzene) λ_{max} (ε_M): 309 (9090), 446 (4600), 1065 (sh, 3690), 1242 (5010) nm (L mol^{-1} cm^{-1}). Anal. Calcd. For $C_{39}H_{29}AlClF_{10}N_3O_2$: C, 56.84; H, 3.55; N, 5.10. Found: C, 56.81; H, 3.73; N, 4.93.

2. Calculations

Calculation S1. Randles-Sevcik equation to test reversibility of redox couples.

$$j_p = 268600n_e^{3/2}D_0^{1/2}C_0v^{1/2}$$

(equation S1)

where j_p is the current density in A/cm^2, n_e is the number of electrons (here n_e = 1), D_0 is the diffusion coefficient (cm^2/s), C_0 is the bulk concentration (mmol/mL) and v is the scan rate (V/s). Straight lines fit to these plots indicate that the electron transfer events can be considered reversible (Figure S11).

Calculation S2. Calculation of Comproportionation Equilibrium Constant (K_c).

$$\Delta G_c° = - RT \ln K_c = - n_eF(\Delta E_{1/2})$$

(equation S2)

where $\Delta G_c°$ is the free energy of the comproportionation reaction ($kcalmol^{-1}$), K_c is the comproportionation equilibrium constant, n_e is the number of electrons, $\Delta E_{1/2}$ is the difference between successive half-wave potentials (V), R is the ideal gas constant (8.314 J mol^{-1} K^{-1}), and F is Faradays constant (96485 J), respectively.

Calculation S3. Application of the Hush Model to estimate electronic coupling (H_{ab1}).

The Hush model, which is best utilized for weakly interacting redox sites or Class II localized electronic systems, gives a lower approximation as to the true electronic coupling between the redox-active sites. [9]

It uses an approximation of r, or the distance between the redox-active sites, which we take as the pyridine nitrogen (N_{py}-N_{py}) distance (Table S6).[10]

$$H_{ab1} = \frac{0.0206}{r}\sqrt{v_{max}\Delta v_{1/2}\,\varepsilon}$$

$$\text{(equation S3)}$$

where v_{max} is the energy of the IV-CT band (in cm^{-1}), ε is the molar absorptivity (M^{-1}cm^{-1}), and $\Delta v_{1/2}$ is the bandwidth at half maximum of the IV-CT band (cm^{-1}), and r is the through-space distance between the two redox sites (Å).

Calculation S4. Application of the Brunchwig-Sutin Model to estimate electronic coupling (H_{ab2}).

Using equations S4 and S5 we obtained values of H_{ab2} which are listed in Table 2 in the main text. ΔG_c^0 (cm^{-1}) is the free energy of the comproportionation reaction to form the mixed valence complex. Assuming non-resonance contributions are small, this free energy is approximately equal to the electronic interaction by delocalization (ΔG_r^0).[11] This free energy ΔG_r^0 can be calculated for a partially delocalized or fully delocalized complex (both are given in Table 1: see Table subscript), and is is taken as the upper limit of the electronic coupling.[10]

For partially delocalized complex $\quad - \Delta G_c^0 \approx - \Delta G_r^0 = \dfrac{2H_{ab2}^{\,2}}{v_{max}}$ $\qquad$ (equation S4)

For fully delocalized complex $\qquad - \Delta G_c^0 \approx - \Delta G_r^0 = 2^{(H_{ab2} - \frac{v_{max}}{4})}$ $\qquad$ (equation S5)
where v_{max} is defined above.

Calculation S5. Application of the parameter Γ to estimate the degree of delocalization of a complex.

Using equation S6, the parameter Γ gives the Robin and Day classification of a mixed-valence system as is described in the main text:

$$\Gamma = 1 - (\Delta v_{1/2})/(\Delta v_{1/2}^{\,o}) \qquad \text{(equation S6)}$$

where $\Delta v_{1/2}$ is the bandwidth at half maximum of the IV-CT band (cm^{-1}), and $\Delta v_{1/2}^{\,o}$ is given by

$$\Delta v_{1/2}^{\,o} = [16RT\,ln2(\lambda)]^{1/2} = [2310\lambda]^{1/2} \qquad \text{at 298K} \qquad \text{(equation S7)}$$

R code. In order to deconvolute the multiple Gaussian distributions in the NIR spectra, non-linear iterative curve fitting using the nonlinear least square[2] (NLS) function in the free-source R was used. The code is provided here for reference.

```
# load data ####
 setwd("C:\\Users\\directory")
 dat <- read.csv("f5i2palcl2.csv", col.names=c("y","x"))
 dat <- dat[!is.na(dat$x) & !is.na(dat$y),] ; dat <- dat[order(dat$x),]
```

```
# Subset to near IR #### To clean data, avoid noise in low energy portion (<4500 cm-1) of spectrum which can influence Gaussian distributions.
  dat <- dat[dat$x >= 4440 & dat$x <= 14500,]

# Plot raw data ####
  plot(dat$x, dat$y, type="l", main="Raw data", xlab="v", ylab="e/v", lwd=2, xlim=rev(range(dat$x)))

# Smooth #### May need to increase "smoothing" depending on noise present in spectrum.
  sampnum <- 25
  y_ma <- filter(dat$y,rep(1/sampnum,sampnum),sides=2)
  plot(y~x, data = dat, type = "l", cex = 0.5, xlim=rev(range(dat$x))) ; points(y_ma~dat$x, data = dat, type = "l", cex = 0.5, col = "red")
  dat$y <- y_ma ; dat <- dat[!is.na(dat$x) & !is.na(dat$y),]

# Drop baseline #### Variable offset may be included in the fit to model a non-zero baseline.
  dat$y <- dat$y - min(dat$y,na.rm=TRUE)

# Gaussian fit ####
  P <- function(x, mean, sd, peakheight){
    peakheight* exp(-(x-mean)^2/(2*sd^2)) }
  p_model <- function(x, peakheights, means, sigmas) {
      rowSums(sapply(1:length(peakheights),  function(i) peakheights[i] * exp(-1* ((x - means[i])^2 / (2*sigmas[i]^2)) ))}
  fit_gauss <- function(y, x, peakheights, means, sigmas, single=FALSE) {
    if(!single){ fit <- nls(y ~ p_model(x, peakheights, means, sigmas), start = list(a=peakheights, b = means, d = sigmas), trace = FALSE,
            control = list(warnOnly = TRUE, minFactor = 1/2048)) }
    if(single){ fit <- nls(y ~ p_model(x, peakheights, means, sigmas), start = list(a=peakheights, b = means, d = sigmas),   trace = FALSE,
            control = list(warnOnly = TRUE, minFactor = 1/2048))}
    return(fit)}

# Get Gaussian fits: give a best guess for vmax, std dev, and height of the peak(s). Add more/fewer Gaussians if necessary (commas to separate).
  plotymax <- 0.5
  peakheights <- c(.15,0.3,0.15,0.05)
  means <-  c(5200,6080,7450,9100)
  sigmas <- c(400,620,440,900)
  g2 <- fit_gauss(y = dat$y, x = dat$x, peakheights = peakheights, means = means, sigmas = sigmas)
  g2coefs <- summary(g2)$coefficients
  nfits <- nrow(g2coefs)/3
  g2coefs <- g2coefs[,"Estimate"] #Contains data: can extract height, location of peak, and standard deviation.

# Plot sum: how well Gaussians match up to your spectrum
  plot(y~x, data = dat, type = "l", main="Summed gaussians", ylim=c(0,plotymax),xlim=rev(range(dat$x)))
  lines(dat$x, predict(g2), lwd = 2, col = "black")

# Plot individuals: individual Gaussians that make up the spectrum
  plot(y~x, data = dat, type = "l", main="Individual gaussians",  ylim=c(0,plotymax), xlim=rev(range(dat$x)),xlab="v",ylab="e/v", col="blue")
  for(k in 1:nfits){lines(x=dat$x,y=P(dat$x,mean=g2coefs[paste("b",k,sep="")],
              sd=g2coefs[paste("d",k,sep="")],peakheight=g2coefs[paste("a",k,sep="")]))    }
```

3. Tables

Table S1. Crystallographic data[a] for the Al complexes: $(_{F5}I_2P^-)(_{F5}I_2P^{2-})Al$ (**2**), $(_{NMe2}I_2P^-)(_{NMe2}I_2P^{2-})Al$ (**3**), $(_{F5}I_2P^-)AlCl_2$ (**4**) and $(_{F5}I_2P^{2-})AlCl(THF)_2$ (**5**).

	2	**3**	**4**	**5**
Formula	$C_{62}H_{26}AlF_{20}N_6$	$C_{70}H_{66}AlN_{10}$ $\bullet 3C_6H_6$	$C_{31}H_{13}AlCl_2F_{10}N_3$ $\bullet THF$	$C_{44}H_{39}AlClF_{10}N_3O_{2.50}$
Crystal size (mm³)	$0.26 \times 0.21 \times 0.12$	$0.52 \times 0.23 \times 0.13$	$0.57 \times 0.50 \times 0.41$	$0.36 \times 0.32 \times 0.21$
Formula wt, g mol⁻¹	1261.87	1308.63	787.43	902.21
Space group	$P2_1/n$	$C2/c$	$P2_1/n$	$P2_1$
a, Å	10.6538(2)	24.1574(4)	13.3802(9)	9.8433(3)
b, Å	21.0744(4)	16.2905(3)	15.1258(9)	10.2481(3)
c, Å	27.7419(6)	19.3440(3)	17.4402(15)	20.4010(6)
α, deg	90	90	90	90
β, deg	90.1860(15)	110.1050(10)	110.9500(10)	103.1935(14)
γ, deg	90	90	90	90
V, Å³	6228.6(2)	7148.7(2)	3296.3(4)	3317.44(15)
Z	4	4	4	4
T, K	90(2)	90(2)	90(2)	90(2)
ρ, calcd. gcm⁻³	1.346	1.241	1.587	1.105
Refl. collected/$2\theta_{max}$	33534/137.938	21026/137.312	42565/55.372	20429/144.828
Unique refl./ $I > 2\sigma(I)$	11446/6478	6497/5191	7707/6403	6458/6108
No. parameters/ restraints	802/0	451/0	469/0	421/0
λ, Å /μ (Kα), cm⁻¹	1.54178	1.54178	0.71073	1.54178
R_1/GOF	0.0618/0.990	0.0526/0.995	0.0319/1.019	0.0361/1.135
wR_2 ($I > 2\sigma(I)$)	0.1447	0.1364	0.0728	0.1257
Residual density, eÅ⁻³	0.380/-0.299	0.395/-0.454	0.515./-0.243	0.509/-0.241

[a] Obtained with graphite-monochromated Cu of Mo Kα ($\lambda = 1.54178$ Å or $\lambda = 0.71073$ Å) radiation. [b]$R_1 = \Sigma||Fo|-Fc||/\Sigma|Fo|$, $wR_2 = \{\Sigma[w(Fo^2-Fc^2)^2]/\Sigma[w(Fo^2)^2]\}^{1/2}$.
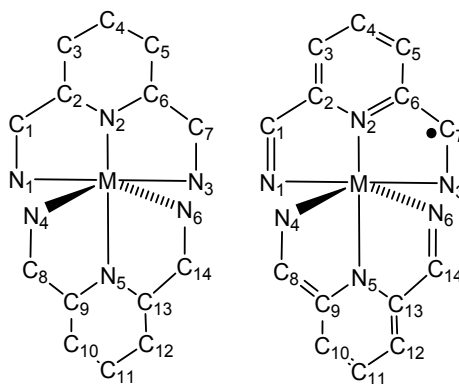
Chart S1. Numbering scheme for compounds used in Tables S2.

Table S2. Selected average interatomic distances (Å) and selected average angles (deg) for the complexes in $[(_{F5}I_2P^-)(_{F5}I_2P^{2-})Al]$ (**2**), $[(_{NMe2}I_2P^-)(_{NMe2}I_2P^{2-})Al]$ (**3**), **4** and **5**.

	2	**3**	**4**	**5**
Al-N$_1$	2.031(3)	2.0193(18)	2.064(1)	2.012(3)
Al -N$_2$	1.940(3)	1.9101(16)	1.902(1)	1.870(3)
Al -N$_3$	2.162(3)	2.0755(18)	2.049(1)	2.008(3)
Al -N$_4$	1.950(3)			
Al -N$_5$	1.874(2)			
Al -N$_6$	2.155(3)			
N$_1$-C$_1$	1.355(4)	1.355(2)	1.321(2)	1.378(4)
N$_3$-C$_7$	1.298(5)	1.323(3)	1.330(2)	1.377(5)
N$_4$-C$_8$	1.424(4)			
N$_6$-C$_{14}$	1.317(5)			
C$_1$-C$_2$	1.417(5)	1.420(3)	1.444(2)	1.385(4)
C$_7$-C$_6$	1.470(5)	1.458(3)	1.440(2)	1.386(4)
C$_8$-C$_9$	1.371(4)			
C$_{14}$-C$_{13}$	1.461(5)			
N$_1$- Al -N$_3$	155.3(1)	156.64(6)	155.41(5)	159.63(13)
N$_4$- Al -N$_6$	159.5(1)			
N$_2$- Al -N$_5$	166.8(1)	179.00(12)		

Table S3. Half-wave potentials for complexes **2**, **3** in THF ($\varepsilon = 7.58$) compared to MeCN ($\varepsilon = 36.6$). Data obtained at 100 mV/s in 0.3M Bu$_4$NBF$_4$ THF and 0.1M Bu$_4$NBF$_4$ MeCN. Data collected in MeCN was tabulated in the main text (Table 1) and is included again here for convenience.

	$E_{1/2}$ (V vs SCE) in THF (in MeCN)		$\Delta E_{1/2}$ (V) [a] in THF (in MeCN)		ΔE_{p} (mV) in THF (in MeCN) [b]	
	2	**3**	**2**	**3**	**2**	**3**
A$^{2+/1+}$	0.75 (0.53)	-0.03 (-0.08)	0.33 (0.33)	0.33 (0.36)	176 (82)	87 (79)
A$^{1+/0}$	0.42 (0.20)	-0.36 (-0.44)	0.68 (0.69)	0.70 (0.65)	146 (86)	87 (71)
A$^{0/1-}$	-0.25 (-0.49)	-1.06 (-1.09)	0.53 (0.38)	0.48 (0.37)	181 (75)	83 (88)
A$^{1-/2-}$	-0.78 (-0.87)	-1.54 (-1.46)	0.94 (0.79)	0.56 (0.47)	167 (93)	97 (93)
A$^{2-/3-}$	-1.72 (-1.66)	-2.10 (-1.93)			120 (56)	192 (86)

[a] $\Delta E_{1/2}$ (V) reported between successive redox couples. [b] Larger values of ΔE_{p} were observed in THF solvent, which is expected in lower dielectric constant solvents as the resistance in the solution increases.[12]

Table S4. Values of K_{c} calculated from experimental CV data in THF. Values for K_{c} in MeCN are reproduced from Table 1 and included in parentheses for convenience.

Comproportionation Equilibrium Reaction	K_{c} values in THF (in MeCN, as in main text)		
	2	**3**	**1**
0/1- + 2-/1- $\rightleftharpoons$ 1-/1-	4.0×10^5 (4.0×10^5)	3.6×10^5 (1.1×10^6)	1.1×10^6 (1.3×10^6)
1-/1- + 2-/2- $\rightleftharpoons$ 2-/1-	2.6×10^{11} (4.8×10^{11})	5.9×10^{11} (9.7×10^{10})	4.8×10^{12} (1.8×10^{13})
2-/1- + 2-/3- $\rightleftharpoons$ 2-/2-	8.0×10^8 (2.7×10^6)	1.5×10^8 (1.8×10^6)	2.9×10^{10} (1.6×10^7)
2-/2- + 3-/3- $\rightleftharpoons$ 2-/3-	8.7×10^{15} (2.4×10^{13})	2.7×10^9 (8.9×10^7)	1.62×10^6 (2.0×10^{10})

Table S5. Electronic Coupling (H_{ab1} and H_{ab2}) for **1** - **3** in various solvents and in various charge states.

	Solvent	H_{ab1} (cm^{-1}) [a]	H_{ab2} (cm^{-1}) [b]
1	Benzene	1780	4660 (4870)
	THF	1590	4680 (4880)
	MeCN	1610	4640 (4860)
2	Benzene	1690	4547 (4622)
	THF	1380	4592 (4659)
	MeCN	1390	4635 (4713)
3	Benzene	1650	4401 (4533)
	THF	2140	4439 (4563)
K$_2$-**1**	THF	2450	4905 (4925)
(K:18-C-6)$_2$-**1**	THF	2180	4284 (4392)
K$_2$-**2**	THF	2390	5303 (5651)
(K:18-C-6)$_2$-**2**	THF	2370	5310 (5650)
K$_2$-**3**	THF	3400	4691 (4695)
(K:18-C-6)$_2$-**3**	THF	2690	4667 (4670)

[a] Calculated from equation S3. [b] Using free energy of comproportionation reaction for partially delocalized (and fully delocalized) system (Table S6, equations S4, S5).

Table S6. Free energy of the comproportionation reaction in MeCN (ΔG_c^0), and the parameters used to determine Class I, II or III: $2H_{ab}/\nu_{max}$
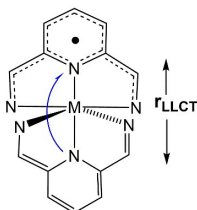
	$r_{LLCT \text{ or } ILCT}$ (Å)	ΔG_c^0 (cm^{-1})	Solvent	$2H_{ab1}/\nu_{max}$	$2H_{ab2}/\nu_{max}$
2	r_{LLCT} = 3.788	-5448	THF	0.36	1.20
LLCT		-5448	Benzene	0.44	1.22
		-5565	MeCN	0.36	1.22
3	r_{LLCT} = 3.887	-5615	THF	0.61	1.30
LLCT			Benzene	0.48	1.31
K$_2$-**2**	r_{LLCT} = 3.788[a]	-7602	THF	0.65	1.53
K$_2$-**3**	r_{LLCT} = 3.887[a]	-4500[b]	THF	0.69	0.96

[a] Estimated r_{LLCT} in **A**$^{2-}$ based on **A** r_{LLCT} distance. [b] Based on non-reversible redox couple [(I$_2$P^{2-})(I$_2$P^{3-})M]$^{2-}$ / [(I$_2$P^{3-})$_2$M]$^{3-}$.

where   Class I: $2H_{ab}/\nu_{max} \ll 1$
                  Class II: $0 < 2H_{ab}/\nu_{max} < 1$
                  Class II/III border: $2H_{ab}/\nu_{max} = 1$

Class III: $2H_{ab}/\nu_{max} > 1$
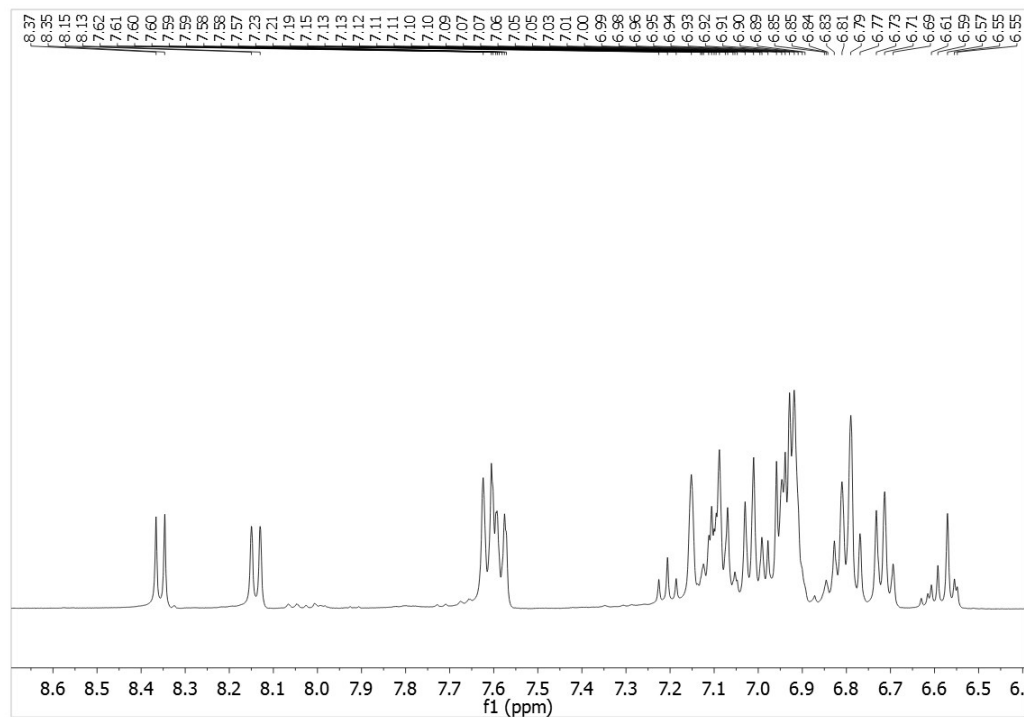
4. Figures

Figure S1: ^{1}H NMR (C$_6$D$_6$, 298K, 400 MHz): $_{F5}$I$_2$P ligand.
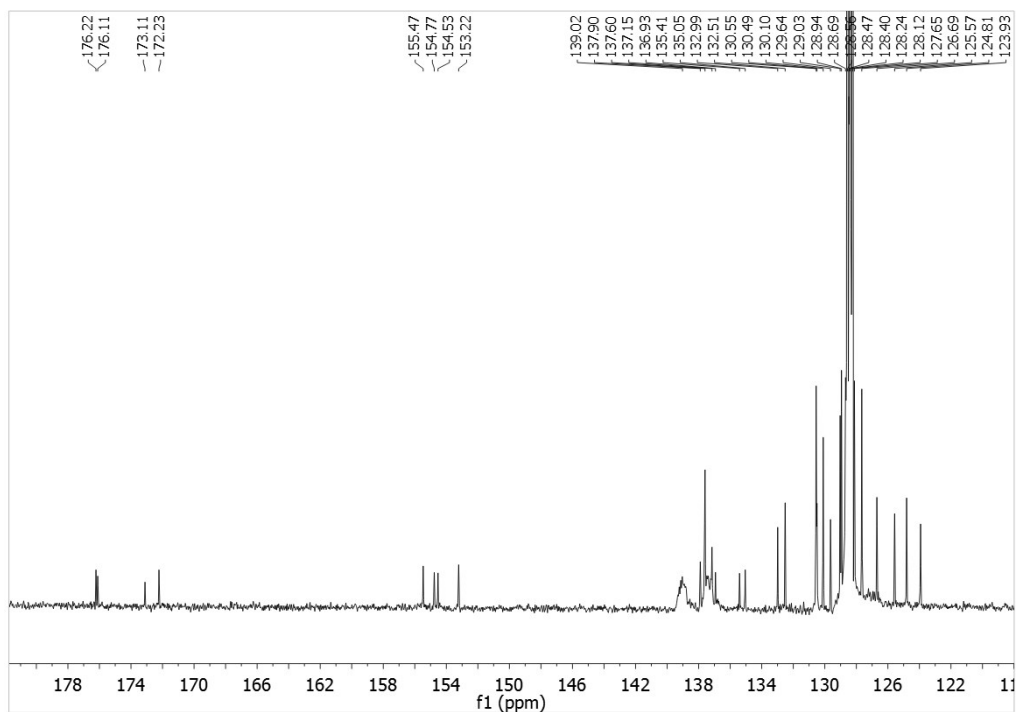
Figure S2: ^{13}C NMR (C$_6$D$_6$, 298K, 150 MHz): $_{F5}$I$_2$P ligand.
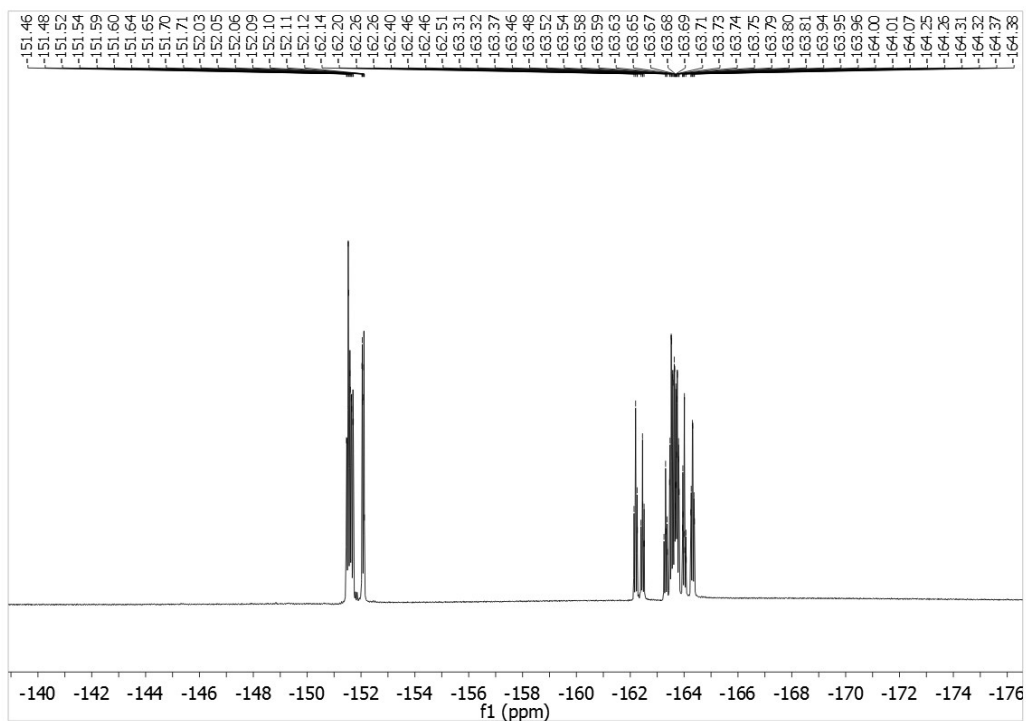
Figure S3: ^{19}F NMR (C$_6$D$_6$, 298K, 377 MHz): $_{F5}$I$_2$P ligand.
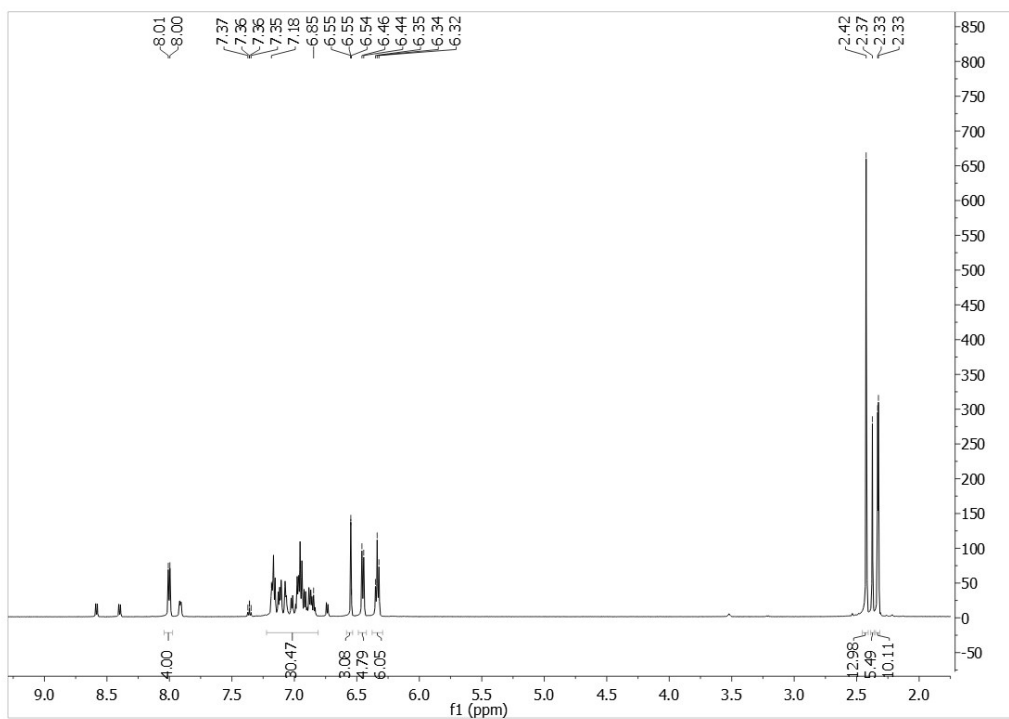
Figure S4: ^{1}H NMR (C$_6$D$_6$, 298K, 400 MHz): $_{NMe2}$I$_2$P ligand.
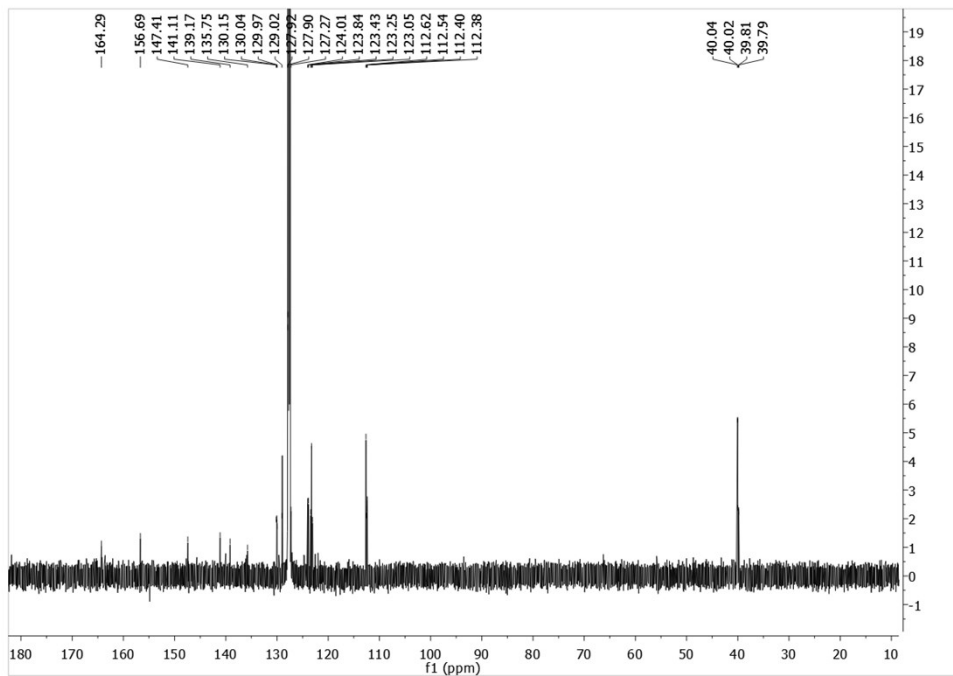
Figure S5: ^{13}C NMR (C_6D_6, 298K, 150 MHz): $_{NMe2}I_2P$ ligand.
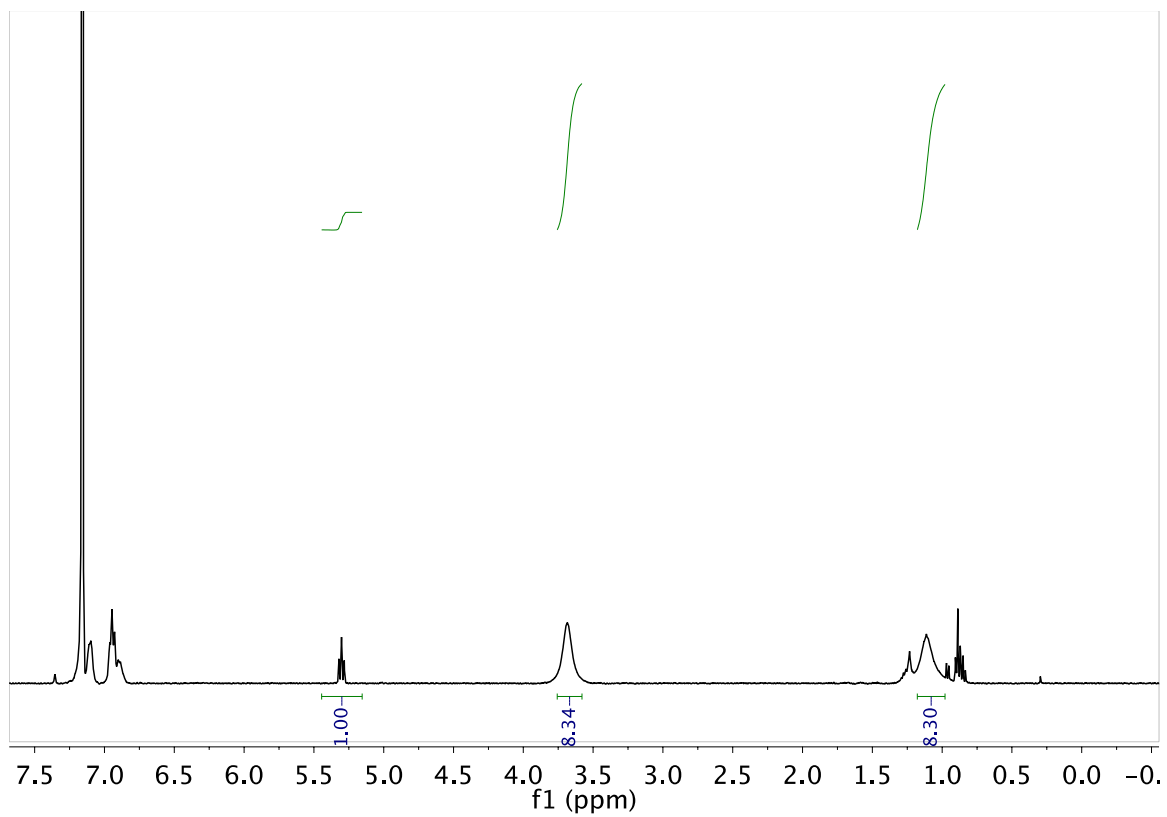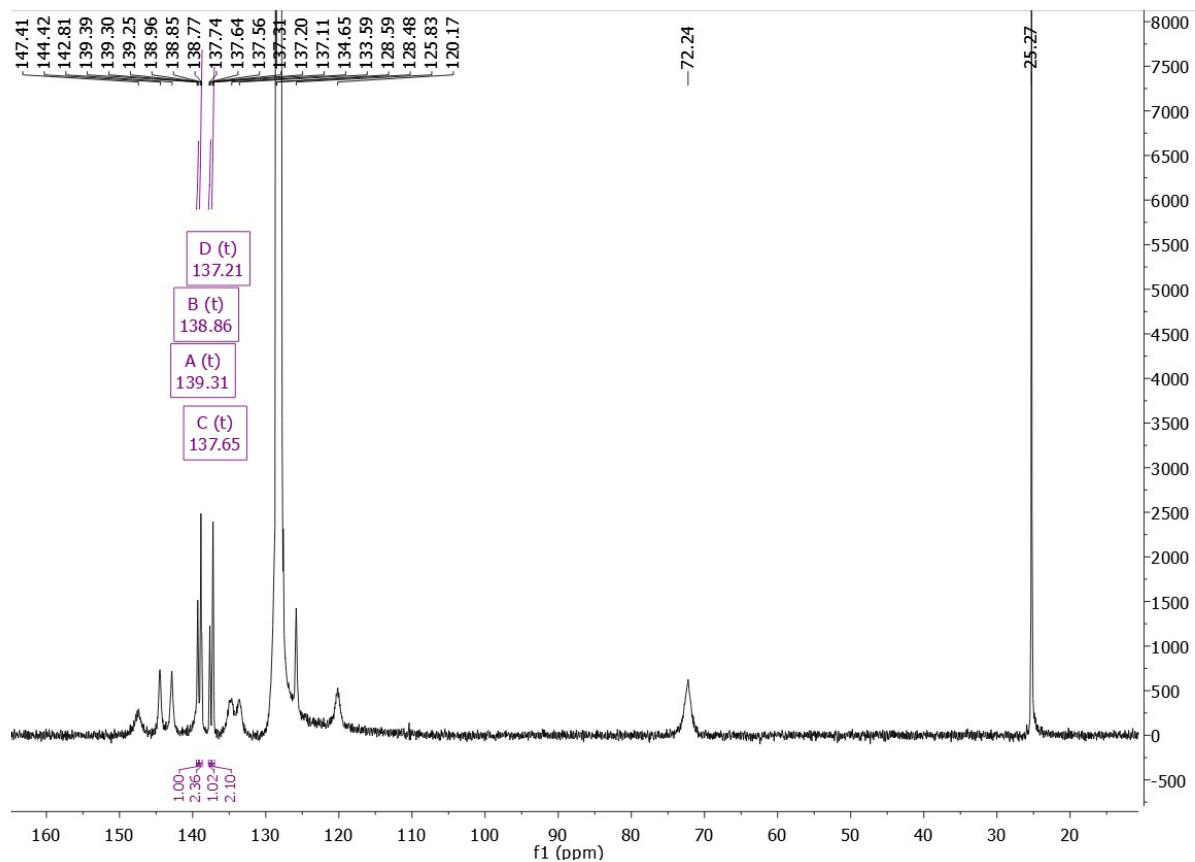
Figure S6: ^{1}H NMR, top (C$_6$D$_6$, 298K, 600 MHz) and ^{13}C NMR (151 MHz, C$_6$D6): **5**.
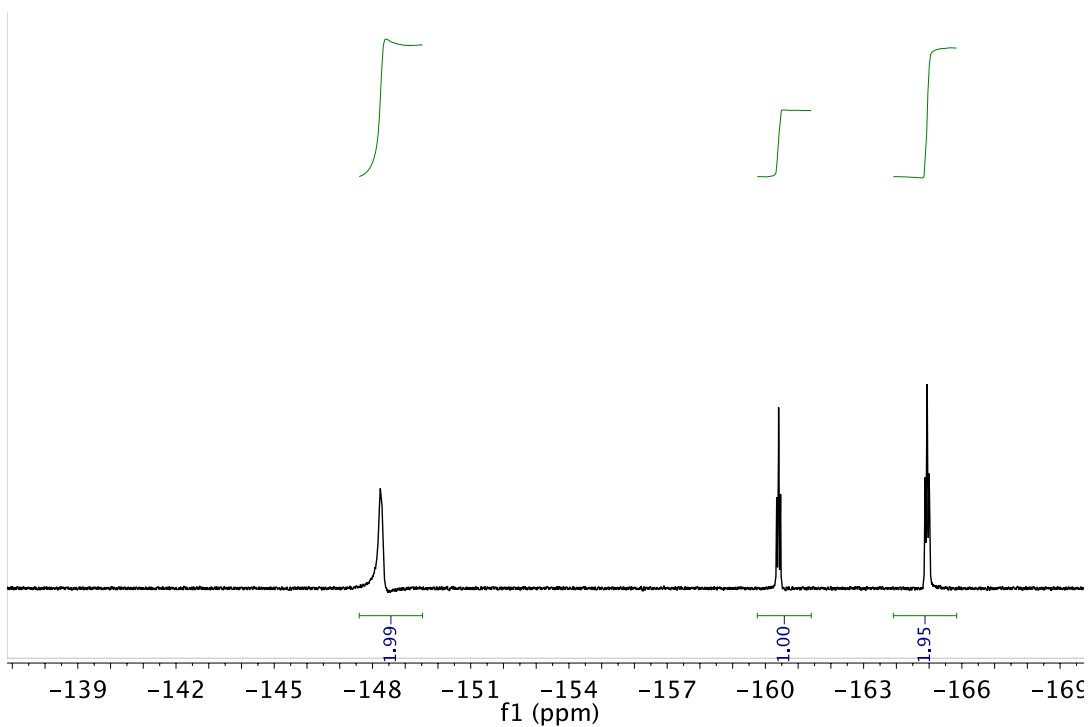
Figure S7: ^{19}F NMR (C$_6$D$_6$, 298K, 377 MHz): **5**.
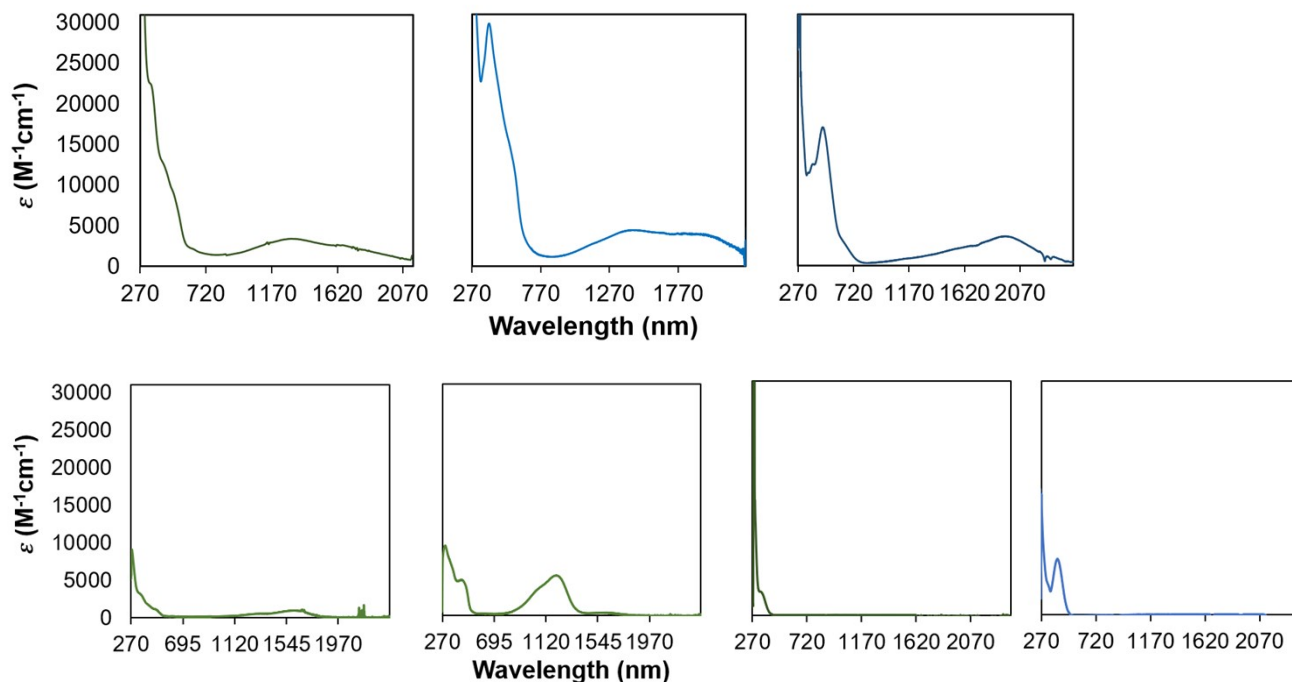
Figure S8. (top) Left to right, UV-vis-NIR spectra of octahedral complexes: **2** (dark green, left), **3** (blue, middle), and **3**$^{2+}$ (dark blue, right) in benzene. (bottom) Left to right, UV-vis-NIR spectra of **4**, **5**, $_{F5}I_2P$, and $_{NMe2}I_2P$, all in benzene.
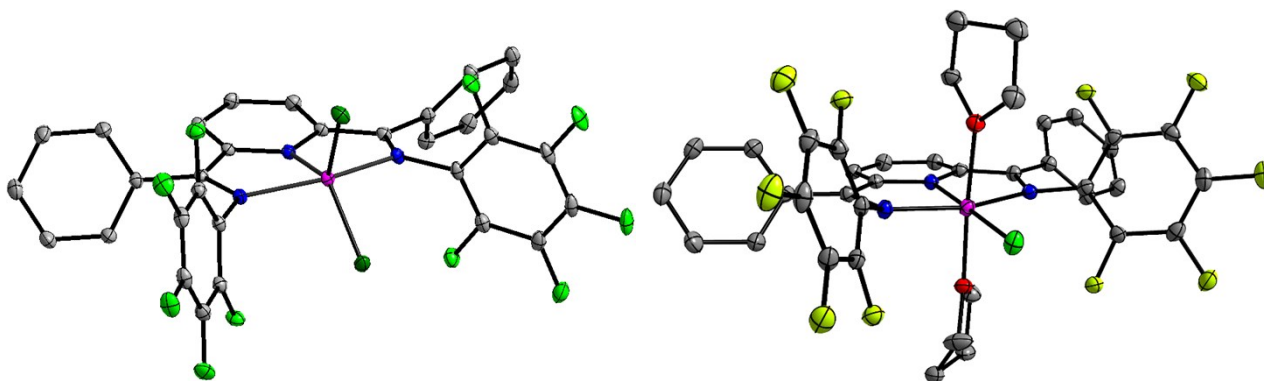
Figure S9. (left) Solid-state structure of ($_{F5}I_2P^-$)AlCl$_2$ in **4**. Dark green, light green, blue, pink and gray ellipsoids represent Cl, F, N, Al and C atoms, respectively. Ellipsoids are shown at 30% probability level. THF solvent molecule and hydrogen atoms have been omitted for clarity. (right) Solid-state structure of ($_{F5}I_2P^{2-}$)AlCl(THF)$_2$ in **5**. Pink, blue, green, red, yellow and grey ellipsoids represent Al, N, Cl, O, F and C atoms, respectively. Ellipsoids shown at 30% probability level.
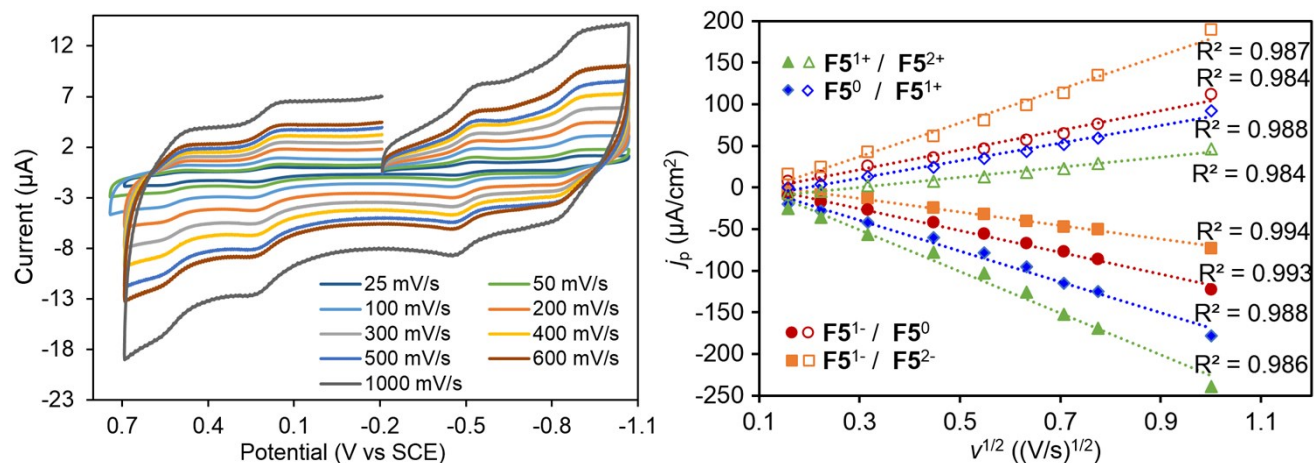
Figure S10. Cyclic voltammetry data to test the reversibility of redox couples of **2** (0.115 mM). Scan rates range from 25 mV/s to 1000 mV/s in 0.1M Bu$_4$NBF$_4$ MeCN (left). Plots of current density (j_p) vs the square root of the scan rate ($v^{1/2}$) (right) were extracted from data in the left figure.
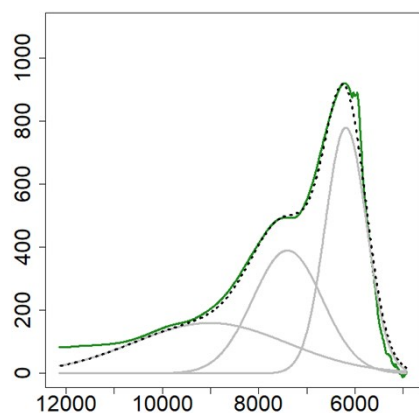
Figure S11. Deconvoluted NIR spectra of **4** in benzene: the dotted black line is the sum of the Gaussian's that make up the spectrum (solid gray lines).
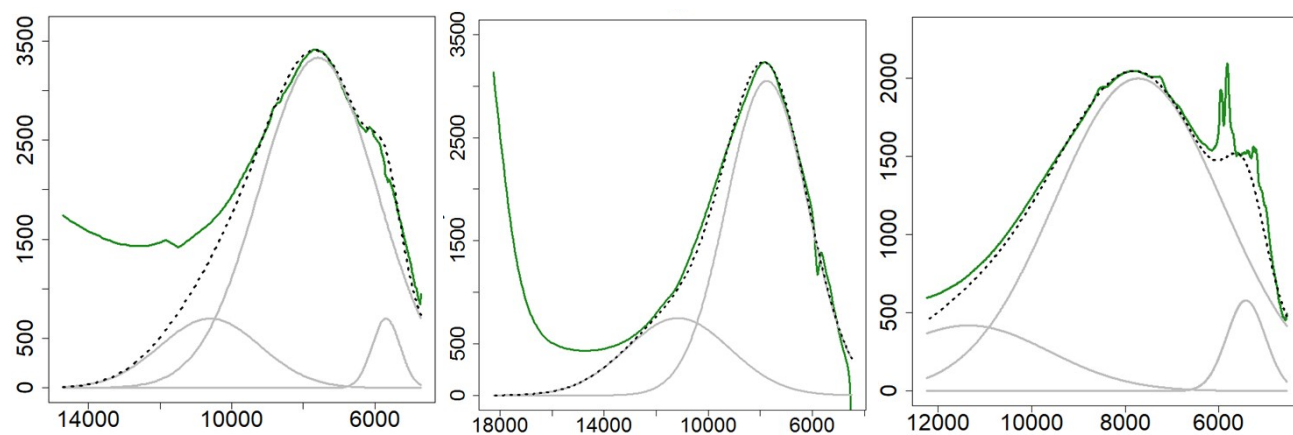
Figure S12. (left) NIR spectra of **2** in benzene; (middle) in THF; (right) in MeCN. The dotted black line is the sum of the Gaussian's that make up the spectrum (solid gray lines).
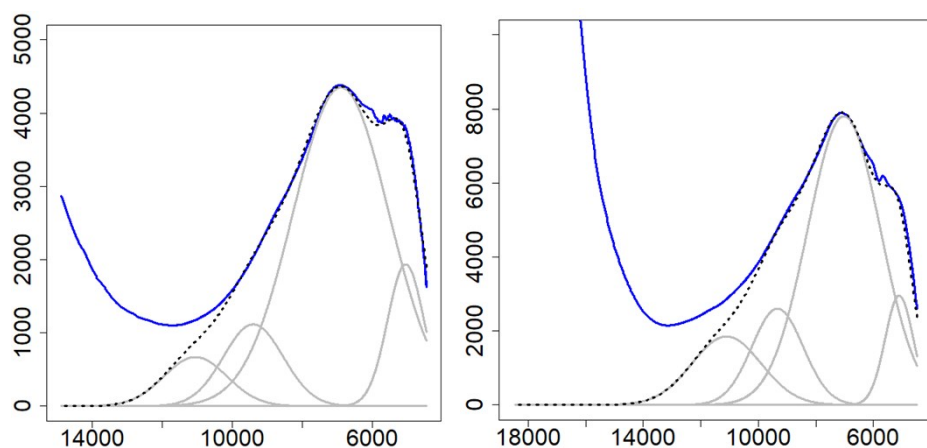
Figure S13. (left) NIR spectra of **3** in benzene and (right) in THF. The dotted black line is the sum of the Gaussian's that make up the spectrum (solid gray lines).
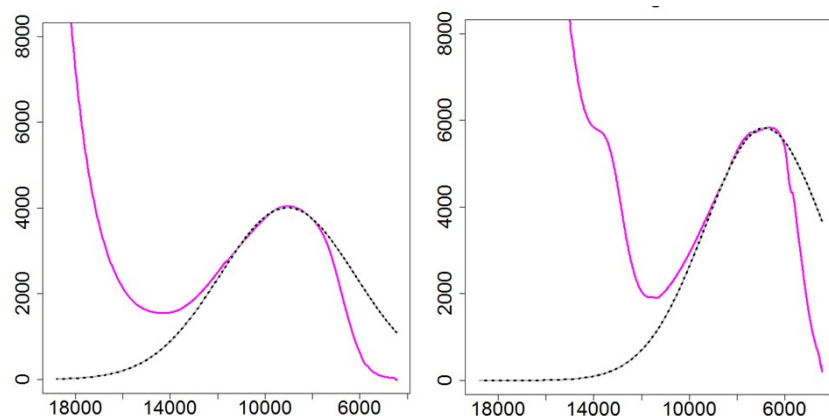
Figure S14. NIR spectra in THF of (left) K$_2$-**1** generated in situ from reaction of **1** with two equivalents of K metal; and (right) and when 18-C-6 is added. The dotted black line is the Gaussian fit to the higher-energy portion of the distribution. When Gaussian distributions are truncated on the lower-energy side, primarily for Class II/III borderline systems, metrics necessary for IV-CT Hush analysis are extracted from the high-energy fit.[4]
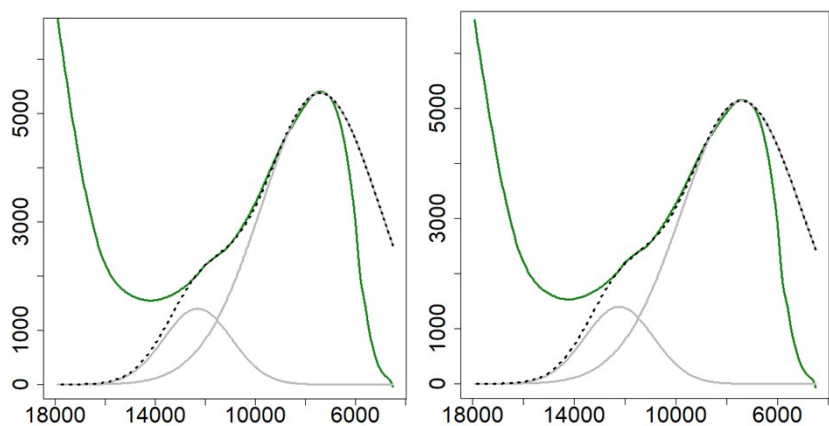
Figure S15. NIR spectra in THF of (left) K$_2$-**2** generated in situ from reaction of **2** with two equivalents of K metal; and (right) and when 18-C-6 is added. The dotted black line is the sum of the Gaussian's that make up the spectrum (solid gray lines).
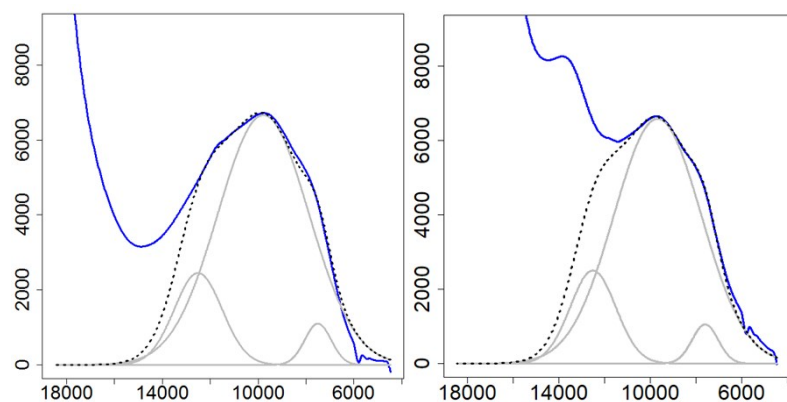
Figure S16. NIR spectra in THF of (left) K$_2$-**3** generated in situ from reaction of **3** with two equivalents of K metal; and (right) and when 18-C-6 is added. The dotted black line is the sum of the Gaussian's that make up the spectrum (solid gray lines).
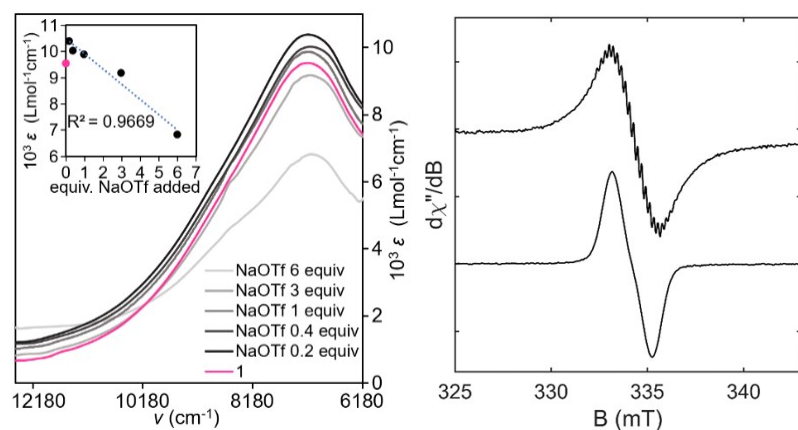
Figure S17. (left) NIR spectra of **1** (pink), titrated with Na$^+$ (gray, black) cations in THF. (right) X-band cwEPR spectra at 298 K of 1 mM **1** (top) and **2** (bottom) in THF.

References and Notes

[1] N. G. Connelly and W. E. Geiger, *Chem. Rev.*, 1996, **96**, 877-910.

[2] D. M. Bates and J. M. Chambers, *Nonlinear Models. Chapter 10 of Statistical Models in S,* ed. J. M. Chambers and T. J. Hastie, Wadsworth & Brooks/Cole, 1992.

[3] R Core Team (2018). R: A language and environment for statistical computing. R Foundation for Statistical Computing, Vienna, Austria. https://www.R-project.org/.

[4] C. Lambert and G. Nöll, *J. Am. Chem. Soc.,* 1999**, 121**, 8434-8442.

[5] J. R. Norris, R. A. Uphaus, H. L. Crespi and J. J. Katz, *Proc. Nat. Acad. Sci.* 1971, **68**, 625-628.

[6] (a) SMART Software Users Guide, Version 5.1, Bruker Analytical X-Ray Systems, Inc.; Madison, WI 1999. (b) SAINT Software Users Guide, Version 7.0, Bruker Analytical X-Ray Systems, Inc.; Madison, WI, 1999. (c) G. M. Sheldrick, SADABS, Version 2.03, Bruker Analytical X-Ray Systems, Inc.; Madison, WI, 2000. (d) G. M. Sheldrick, SHELXTL Version 6.12, Bruker Analytical X-Ray Systems, Inc.; Madison, WI, 1999. (e) International Tables for XRay Crystallography, 1992, Vol. C., Dordrecht: Kluwer Academic Publishers.

[7] N. Kleigrewe, W. Steffen, T. Blömker and G. Kehr, *J. Am. Chem. Soc.* 2005, **127**, 13955–13968.

[8] A. Arnold, T. J. Sherbow, R. I. Sayler, R. D. Britt, E. J. Thompson, M. T. Muñoz, J. C. Fettinger and L. A. Berben, *J. Am. Chem. Soc.*, 2019, **141**, 15792-15803.

[9] a) G. C. Allen and N. S. Hush, *Prog. Inorg. Chem.*, 1967, **8**, 357-389. (b) M. B. Robin, P. Day, *Adv. Inorg. Chem. Radiochem.*, 1968, **10**, 247-422. (c) N. S. Hush, *Electrochim. Acta,* 1968**, 13**, 1005-1023.

[10] S. F. Nelsen, H. Q. Tran and M. A. Nagy, *J. Am. Chem. Soc.,* 1998, **120**, 298-304.

[11] B. S. Brunschwig and N. Sutin, *Coord. Chem. Rev.*, 1999, **187**, 233-254.

[12] Bard, A. J. *Electroanalytical Chemistry: A Series of Advances*; CRC Press, 1990.